ACS SENSORS

Article

Cite This: ACS Sens. XXXX, XXX, XXX−XXX

pubs.acs.org/acssensors

Wearable Electrochemical Microneedle Sensor for Continuous Monitoring of Levodopa: Toward Parkinson Management

K. Yugender Goud,[†] Chochanon Moonla,[†] Rupesh K. Mishra,[†] Chunmei Yu,[†] Roger Narayan,[‡] Irene Litvan,[*,§] and Joseph Wang[*,†]

[†]Department of NanoEngineering and [§]Department of Neurosciences, University of California San Diego, 9500 Gilman Drive #0948, La Jolla, California 92093, United States

[‡]Joint Department of Biomedical Engineering, University of North Carolina and Carolina State University, Raleigh, North Carolina 27695-7115, United States

Supporting Information

ABSTRACT: Levodopa is the most effective medication for treating Parkinson's disease (PD). However, because dose optimization is currently based on patients' report of symptoms, which are difficult for patients to describe, the management of PD is challenging. We report on a microneedle sensing platform for continuous minimally invasive orthogonal electrochemical monitoring of levodopa (L-Dopa). The new multimodal microneedle sensing platform relies on parallel simultaneous independent enzymatic-amperometric and nonenzymatic voltammetric detection of L-Dopa using different microneedles on the same sensor array patch. Such real-time orthogonal L-Dopa sensing offers a built-in redundancy and enhances the information content of the microneedle sensor arrays. This is accomplished by rapid detection of L-Dopa using square-wave voltammetry and chronoamperometry at unmodified and tyrosinase-modified carbon-paste microneedle electrodes, respectively. The new wearable microneedle sensor device displays an attractive analytical performance with the enzymatic and nonenzymatic L-Dopa microneedle sensors offering different dimensions of information while displaying high sensitivity (with a low detection limit), high selectivity in the presence of potential interferences, and good stability in artificial interstitial fluid (ISF). The attractive analytical performance and potential wearable applications of the microneedle sensor array have been demonstrated in a skin-mimicking phantom gel as well as upon penetration through mice skin. The design and attractive analytical performance of the new orthogonal wearable microneedle sensor array hold considerable promise for reliable, continuous, minimally invasive monitoring of L-Dopa in the ISF toward optimizing the dosing regimen of the drug and effective management of Parkinson disease.

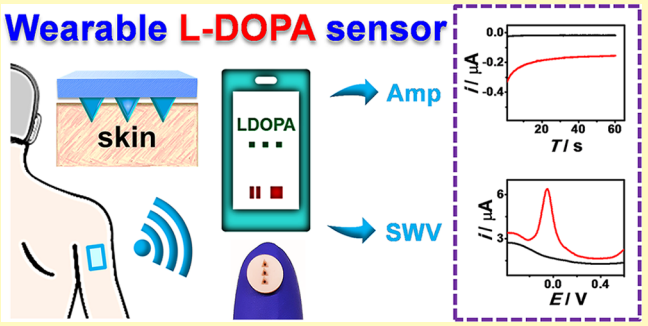

KEYWORDS: *microneedle, L-Dopa, Parkinson disease, wearable sensor, orthogonal detection, minimally invasive monitoring, biosensor*

Parkinson's disease (PD) is the second most common neurodegenerative disorder after Alzheimer's disease.[1,2] PD leads to disability, affects patients' and families' quality of life and finances, and increases healthcare cost.[2] An estimated 7 to 10 million people worldwide have PD, including over 1 million Americans with 60,000 Americans being diagnosed every year.[3]

Since its introduction in the 1960s, levodopa (L-Dopa), the precursor of dopamine, has remained the most effective anti-Parkinson's drug.[4] Indeed, L-Dopa remains the gold standard for treating the disease for over five decades. L-Dopa is converted into dopamine, which is the neurotransmitter lost in PD and is critical for the motor pathways' function.[4] L-Dopa therapy is thus commonly used to increase dopamine concentrations for treating PD symptoms. However, with disease progression, the increasing dopamine neuronal loss along with the L-dopa's short half-life leads to a narrow therapeutic window and patients' experience of symptomatic motor and nonmotor fluctuations. To maintain the same therapeutic effect, L-Dopa doses must be adjusted avoiding the consequences of low doses leading to symptoms, such as Parkinsonism, anxiety, and depression or higher concentrations that result in dyskinesias, psychosis, orthostatic hypotension, etc.[5,6] Healthcare professionals rely on patients to report symptoms, but most patients have difficulty distinguishing between dyskinesias or tremors and/or the time of their antiparkinsonian medication intake.

To address these issues and provide the greatest improvement in motor function, there are urgent needs for a reliable

Received: June 20, 2019
Accepted: July 31, 2019

DOI: 10.1021/acssensors.9b01127
ACS Sens. XXXX, XXX, XXX−XXX

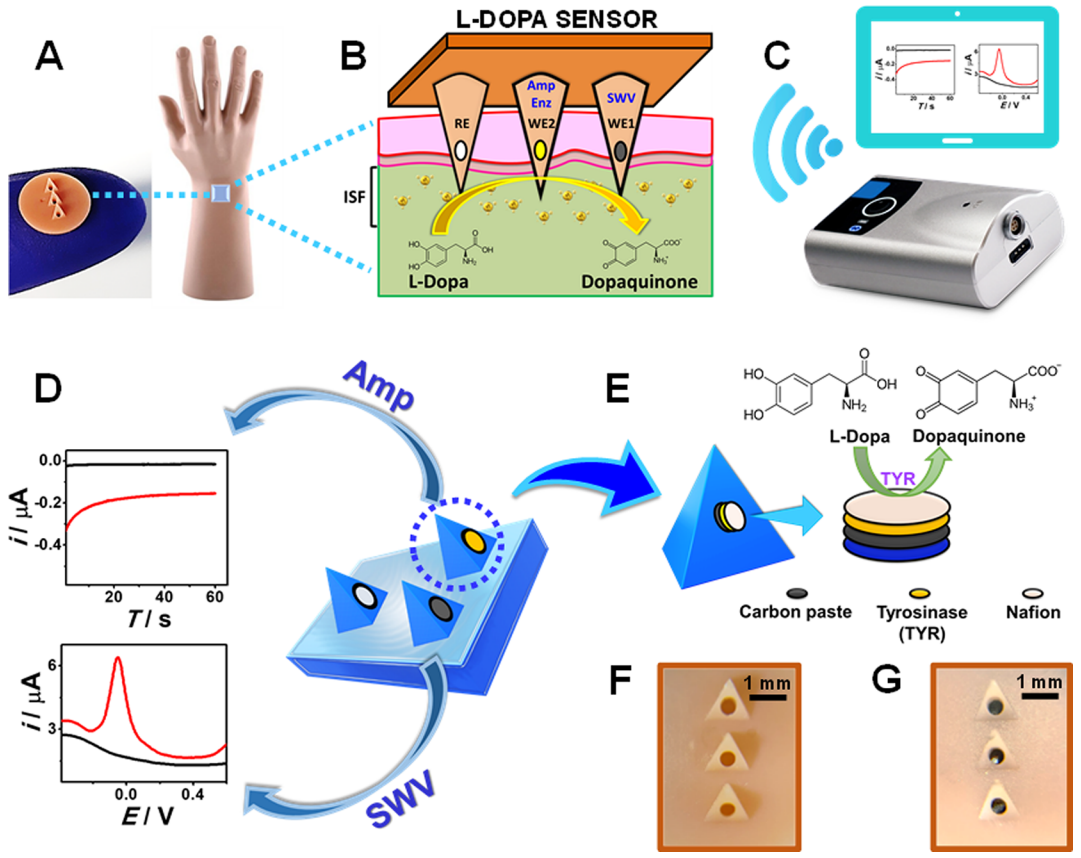

Figure 1. Microneedle sensor for L-Dopa detection; schematic representation of (A) mannequin hand wearing the microneedle sensor and (B) the microneedle sensor for L-Dopa monitoring in ISF. (C) Portable wireless electroanalyzer enabled with wireless data transmission to the smart device; (D) schematics of the microneedle sensor platform, illustrating three electrodes used for L-dopa sensing using SWV and amperometry; (E) microneedle sensor with the corresponding reagent layers, including the CP, tyrosinase, and Nafion layer. (F, G) Actual optical images of microneedles before and after packing with CP (scale bar, 1 mm).

sensing device to provide timely individualized feedback on the proper L-Dopa dosing regimen in a decentralized and rapid fashion. Measurement of PD patients' L-Dopa concentrations in biofluids would not only allow better management of middle and late PD stages but can also improve the management of PD at early stages. In view of the fact that administration of high doses of L-Dopa at early PD stages leads to earlier development of PD fluctuations, knowledge of L-Dopa concentrations will allow the use of lower L-Dopa doses at early stages, which will likely delay the onset of fluctuations.

Plasma levels of L-dopa are commonly measured using high-performance liquid chromatography (HPLC) and correlate accurately with motor symptoms' severity.[7,8] However, HPLC is not a viable method for timely adjustment of L-Dopa dosage because of its slow delivery of the results and high costs.[9] Recent efforts have demonstrated the potential of electrochemical techniques for in vitro measurements of L-Dopa.[10−17] This activity relied on the use of electrodes modified with a variety of nanoscale materials toward accelerating the L-Dopa oxidation process, including carbon nanotube (CNT)−chitosan−glassy carbon electrodes (GCE),[10] CNT−chitosan screen-printed electrodes (SPCE),[11] CNT−gold nanoparticle−graphite electrodes,[10] SWCNT-GCE,[12] GCE-MWCNT−polypyrrole,[13] GCE-MWCNT−nickel hydroxide nanoparticles (NPs),[14] 3D graphene foam,[15] TiO_2 nanofiber−graphene oxide,[16] and nickel hexacyanoferrate−Au NP−graphite.[17] Considering these extensive laboratory-based electrochemical sensing studies, there is an immense need and promise for developing a wearable electrochemical sensing platform for continuous monitoring of L-Dopa in a Parkinson's patient's blood or other physiologically relevant fluids.

Wearable sensor technology has advanced rapidly in recent years to provide tremendous opportunities for improving personalized healthcare.[18−23] A number of wearable sensors have been developed to monitor motor fluctuations of PD patients and the severity of Parkinsonian symptoms.[24] However, no attempts have been made to develop wearable chemical sensors for monitoring these patients toward improved management of PD. Among the variety of recently introduced wearable chemical sensing platforms, microneedle sensors have received considerable attention for simple, rapid, continuous, painless, minimally invasive transdermal sensing of various biomarkers in the body interstitial fluid (ISF). Microneedle arrays have thus been developed for the continuous real-time monitoring of clinically relevant biomarkers,[25−27] such as glucose,[28−37] lactate,[38−41] alcohol,[42] potassium ion,[43] and organophosphate.[44] So far, there is no attempt made for using microneedles for monitoring L-Dopa in ISF.

This article describes a new orthogonal electrochemical/biocatalytic microneedle sensor array strategy toward continuous minimally invasive monitoring of L-Dopa. This orthogonal dual-sensing platform can provide rich electrochemical information toward measurements of the target L-

DOI: 10.1021/acssensors.9b01127
ACS Sens. XXXX, XXX, XXX−XXX

Dopa analyte compared to common single-modality sensing routes. The two-working electrode microneedle array was constructed by packing hollow microneedles with different carbon paste (CP) electrode transducers. As illustrated in Figure 1, direct (nonenzymatic) anodic L-Dopa detection was carried out using square-wave voltammetry (SWV) using microneedle WE1, while a tyrosinase (TYR)-based biocatalytic detection was performed at the neighboring enzyme-paste microneedle electrode (WE2) using chronoamperometric measurements of the corresponding dopaquinone product. Both microneedle working electrodes offered high sensitivity and selectivity toward the L-Dopa target along with good stability and a linear current response. The attractive performance and potential wearable applications of the new microneedle sensor array have been demonstrated in skin-mimicking phantom gel and upon penetration through a mice skin. Such a combination of two independent detection processes onto a single microneedle platform greatly enhances the available analytical information and offers considerable promise for continuous monitoring of L-Dopa and for increasing the power of wearable electrochemical sensors in general. Surprisingly, despite the considerable analytical potential of such a multimodal sensing format, the coupling of several distinct independent processes in a single wearable device has rarely been applied for on-body electrochemical sensors. The new microneedle orthogonal sensing concept extracts further analytical information and leads to a built-in redundancy and cross-check in case of potential interferences on one of the detection modes. Such orthogonal microneedle sensing can be extended for the continuous analysis of other biomarkers present in ISF. Ultimately, the developments described in the following sections will lead to a closed-loop feedback sensor delivery system that relies on the L-Dopa blood level as a feedback signal for adjusting the L-Dopa dose, which will lead to improved treatment and management of PD symptoms and enhanced quality of life of patients.

EXPERIMENTAL SECTION

Chemicals. The enzyme tyrosinase (from mushroom, EC 1.14.18.1, 1679 units mg^{-1}), 3,4-dihydroxy-L-phenylalanine (L-Dopa), ascorbic acid (AA), uric acid (UA), theophylline, tyrosinase, potassium phosphate monobasic (KH_2PO_4), potassium phosphate dibasic (K_2HPO_4), sodium chloride, potassium chloride, sucrose, sodium gluconate, Nafion, calcium chloride (anhydrous), magnesium sulfate (anhydrous), albumin from bovine serum (BSA), γ-globulins from bovine blood, and mineral oil were purchased from Sigma-Aldrich, and ethyl alcohol was obtained from Decon Labs (Austin, U.S.A.). Agarose was procured from MCB reagents (Cincinnati, Ohio), and graphite powder (crystalline, 99%) was purchased from Alfa Aesar (Ward Hill, MA) and used without further modification.

Instrumentation, Procedure, and Microneedle-Array Fabrication. All electrochemical measurements (SWV and chronoamperometry) were performed using a PalmSens EmStat3 handheld potentiostat controlled by PSTrace software version 5.5. Microneedle photographs were taken using a digital camera (Nikon, D7000). Square-wave voltammetric and chronoamperometric experiments were carried out in a 0.1 M PB solution (pH 7.4) and artificial ISF solution. The L-Dopa stock solutions were prepared in PB. SWV was carried out over the potential range −0.4 to 1.0 V (vs Ag/AgCl) for 30 s. Chronoamperometry experiments were carried out for 60 s using an applied potential of 0.1 V (PB solution) or 0.3 V (for artificial ISF). The L-Dopa sample solution (30 μL of droplets) was placed on the surface of the inverted microneedle electrode array throughout the electrochemical measurements.

The microneedle electrodes were prepared similar to our previous studies.[40] The trilateral base of the microneedle sensor contains 1 × 3 hollow microneedle arrays, which were in a pyramidal shape. The height of the hollow microneedles was 1500 μm with a diameter of 425 μm. A vertical cylindrical hole was intentionally kept at one side of the pyramid microneedle structure. The interspace between each microneedle array was kept 1 mm.

L-Dopa sensing was carried out using a three-hollow microneedle array. Two of these hollow microneedles were packed with freshly prepared CP with an unmodified paste in WE1 and the enzyme-containing paste in WE2. The third electrode was modified with a Ag wire and used as a reference electrode (RE). We tested also an additional carbon-paste counter electrode during our analysis, but this addition did not provide any improvement in the sensor response and hence was not used in subsequent work. Each hollow microneedle electrode had a surface area of 0.002 cm^2. The CP used in WE1 was prepared by mixing 65 wt % graphite powder and 35 wt % mineral oil. For the enzymatic WE2 preparation, the paste composition included 55 wt % graphite powder, 10 wt % tyrosinase mushroom enzyme, and 35 wt % mineral oil. Following the CP packing, the excess paste was carefully removed from the surface using a surgical blade followed by smoothing the microneedle surface with wax paper. Electrical contacts were established from the rear side of the packed microneedles by connecting with stainless Cu wires. These wires were attached using conductive silver epoxy ink and cured at 85 °C for 10 min before packing and placing fresh paste on the microneedle surface for each experiment.

In Vitro Evaluation. The electroanalytical performance of the microneedle sensor has been performed in 0.1 M PB solution (pH 7.4) and artificial ISF (pH 7.4). The artificial ISF solution was prepared by following the reported literature.[45] SWV experiments were carried out in the applied potential scan between −0.4 to 1.0 V (vs Ag/AgCl). Chronoamperometry experiments were performed for 60 s at 0.1 V for PB solution and 0.3 V for artificial ISF. The stability of the enzyme and nonenzymatic microneedle sensors were performed by conducting repetitive experiments of SWV and chronoamperometry experiments for a prolonged period (up to 100 min). The selectivity of both microneedle sensors was tested in the presence of possible interferences, such as ascorbic acid, uric acid, tyrosine, and theophylline. During these interference studies, the enzyme and nonenzymatic sensing electrodes were covered with 2 μL of 1% Nafion solution that led to an anti-interference barrier. Carbidopa (C-Dopa) and L-Dopa cross studies were performed on nonenzymatic carbon paste microneedle electrodes. Biofouling studies have been carried out on nonenzymatic microneedle CP electrodes in the presence of BSA, ascorbic acid, uric acid, and globulin proteins. All other solutions were prepared using ultrapure deionized water.

Preparation of Phantom Gel Mimicked Skin. To mimic the human skin, agarose phantom gel was prepared by following the recently published work on microneedles.[46,47] Initially, 140 mg of agarose was dissolved in 10 mL of PBS (1.4%) and stirred at 120 °C in a glass vial until complete dissolution was obtained. Subsequently, the homogenous agarose liquid was poured into the petri dish and allowed to solidify. Subsequently, three solutions containing different L-Dopa concentrations were dispensed onto the individual petri dishes and were allowed to diffuse for 60 min at room temperature. During the phantom hydrogel experiments, the microneedle sensor array was tested within the phantom gel, allowing 1 min of contact of the needle tips with the gel followed by the SWV and amperometric detection of the L-Dopa.

Ex Vivo Evaluation. The utility of the microneedle sensor was examined also ex vivo by penetrating mice skin placed on top of an artificial ISF solution containing L-Dopa. The mice skin was collected and stored at −20 °C. Later, the mice skin specimen was cooled down to room temperature and cut into the small pieces. The microneedle was pierced carefully into the small mice skin pieces. The ex vivo L-Dopa testing was carried out with a compartment filled with artificial ISF. Then, the mice skin-penetrated microneedle was placed on the top of the compartment, allowing the microneedle sensor tips for contact with the artificial ISF. SWV and chronoamperometric experiments were subsequently performed using optimal parameters.

DOI: 10.1021/acssensors.9b01127
ACS Sens. XXXX, XXX, XXX−XXX

RESULTS AND DISCUSSION

Principle and Design of the Microneedle Sensor Array. The new microneedle sensor array relies on parallel independent electrochemical measurements of L-Dopa using enzymatic-amperometric measurements and direct (non-enzymatic) square-wave voltammetric detection (Figure 1B). One of the hollow microneedle electrodes, labeled WE1, contained an unmodified carbon-paste voltammetric electrode, while the second microneedle, labeled WE2, contained the enzyme (TYR)-modified paste. The Ag wire served as a reference electrode in the two-electrode sensing without a counter electrode. A schematic representation of electrochemical detection of L-Dopa using the enzymatic (chronoamperometry) and nonenzymatic (SWV) microneedle sensors is presented in Figure 1D. In the case of the nonenzymatic sensor, a rapid square-wave scan leads to direct oxidation of the target L-Dopa. In parallel, biocatalytic oxidation of L-Dopa is carried out at the tyrosinase enzyme embedded CP microneedle electrode with the dopaquinone product being detected amperometrically (Figure 1D). Such a pair of orthogonally measured electrochemical signals (redox and biocatalytic) can capture potential interferences, such as those of carbidopa upon the enzymatic sensor (but not on the voltammetric one). Images of the three hollow microneedles, before and after packing with the corresponding paste electrode materials, are displayed in Figure 1F,G. A schematic illustration of the biocatalytic reaction of L-Dopa by the immobilized tyrosinase enzyme is presented in Figure 1E. Note also the Nafion coating, which serves as a permselective protective layer that imparts high selectivity and stability. The resulting enzymatic and nonenzymatic microneedle sensors were evaluated first in PB solution (pH 7.4) followed by testing in artificial ISF and in a tissue-mimicking phantom gel.

Optimization and Characterization of the Microneedle L-Dopa Sensors. SWV parameters, such as frequency, amplitude, and potential step, play an important role while analyzing the electrocatalytic reaction of drug molecules. A wide range of frequencies (10−30 Hz) and amplitudes (10−50 mV) was tested and compared (Figure S1A,B) with a 20 Hz frequency and 0.05 V amplitude offering the most favorable SWV performance of the unmodified carbon-paste microneedle sensor.

Subsequently, the thickness of the permselective Nafion layer (1% w/v in ethanol) was optimized toward the highest sensitivity and selectivity. Different volumes of Nafion (1, 2, and 3 μL) were drop cast on the working electrode surface and recorded the SWV at 50 μM L-Dopa concentrations. As shown in Figure S2, the oxidation peak current of L-Dopa was higher at 2 μL of Nafion coating compared to the other tested volumes. Subsequently, the experiments were conducted to optimize the accumulation time by performing the SWV scans following 2, 4, and 6 min incubation. The results shown in Figure S3 indicate that the anodic peak current increases upon increasing the accumulation time, reflecting electrostatic interaction with the coating. Subsequent analytical experiments were thus carried out using the 2 μL Nafion coating and following 1 min accumulation.

The analytical performance of the nonenzymatic microneedle sensor was examined toward the detection of L-Dopa by recording SWV in a phosphate buffer solution. A broad dynamic range between 5 and 300 μM L-Dopa (Figure S4A) was tested. The optimized parameters (potential range, −0.4 to 1.0 V vs Ag/AgCl using a frequency of 20 Hz and amplitude of 50 mV) were used to perform these experiments. As illustrated in Figure S4A, a well-defined baseline was obtained followed by distinct voltammograms of L-Dopa oxidation observed through the calibration range. The L-Dopa oxidation peak was obtained at a very low potential of −0.05 V potential. The resulting calibration plot is shown in the inset of Figure S4A. Two linear ranges were observed in the concentration range from 5 to 100 μM and 100 to 300 μM with correlation coefficients (R^2) of 0.989 and 0.9798, respectively (RSD 4.0%, n = 3) that permit an appropriate analysis of these micromolar L-Dopa concentrations. Simultaneously, the analytical response of the enzymatic microneedle biosensor toward L-Dopa was evaluated in the range between 20 and 300 μM by recording the chronoamperometric responses in a phosphate buffer. The current was sampled for 60 s at an applied potential of 0.1 V (vs Ag/AgCl) reference electrode. Figure S4B displays chronoamperograms for increasing L-Dopa concentrations (20 to 300 μM) along with the corresponding calibration plot (inset). A well-defined amperometric response is observed over the entire concentration range with high linearity (20 to 300 μM) and a correlation coefficient of 0.998 (RSD = 3.3%, n = 3). These results showed that the biosensor retains a wide dynamic concentration range.

Continuous monitoring of the L-Dopa level is a significant task in the medical diagnosis of a Parkinson's patient. There is no such existing method; hence, the microneedle sensor has been further studied in artificial ISF for the detection of L-Dopa. Both enzyme and nonenzymatic microneedle sensors were analyzed for the continuous evolution of the antiparkinson drug (L-Dopa) in ISF. Nonenzymatic microneedles were tested using the optimal SWV parameters (potential range, −0.4 to 1.0 V vs Ag/AgCl using a frequency of 20 Hz and amplitude of 50 mV). Figure 2A displays the SWV response for successive additions of 20 μM L-Dopa in artificial ISF over a wide dynamic range between 20 and 360 μM along with the corresponding calibration plot (inset). A well-defined L-Dopa oxidation peak is observed with a peak potential of 0.2 V. The anodic peak current increases linearly with the L-Dopa concentration up to 160 μM followed by a slight curvature at higher concentrations (see inset for the corresponding calibration plot). Additionally, the tested sensor displayed good reproducibility and sensitivity (0.037 μA/μM) with a correlation coefficient of 0.988 (RSD = 3%, n = 3).

Good operational stability is a paramount requirement for the minimally invasive microneedle sensors. As illustrated in Figure 2C, the L-Dopa microneedle sensor offers a highly stable and reproducible SWV response. For example, an initial stability test was carried out over a 110 min period by recording the SWV response for 100 μM L-Dopa in artificial ISF using 10 min time intervals. A similar response was obtained from each analysis, which signifies good reproducibility of the sensor performance (SD = 2.5, n = 11). Such a stable and reproducible response supports the exploration of the nonenzymatic SWV microneedle sensor for continuous monitoring of L-Dopa.

The analytical response of the enzymatic microneedle biosensor toward L-Dopa was evaluated first by recording chronoamperometry responses in artificial ISF over the 20 to 300 μM range. The current was sampled for 60 s at an applied working potential of 0.3 V (vs Ag/AgCl reference electrode). Figure 2B displays the chronoamperometric response of the TYR-microneedle biosensor for successive 20 μM L-Dopa

DOI: 10.1021/acssensors.9b01127
ACS Sens. XXXX, XXX, XXX−XXX

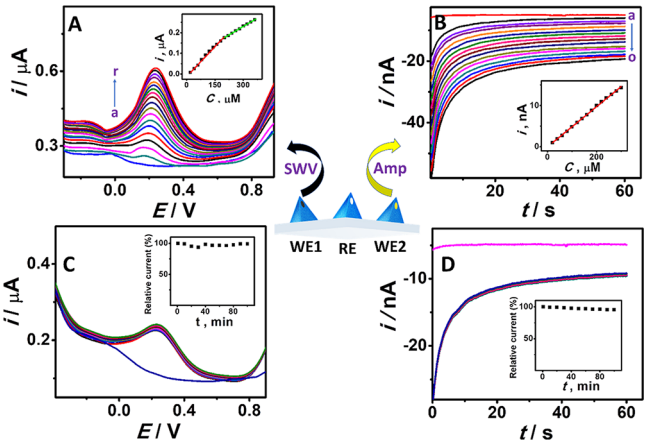

Figure 2. Dual functionality microneedle sensors for L-Dopa detection. (A) Square-wave voltammograms for L-Dopa in artificial ISF over the f 20−360 μM concentration range with 20 μM increments using the unmodified carbon-paste microneedle sensor; inset shows the resulting calibration plot. SWV potential range −0.4 to 1.0 V (vs Ag/AgCl) using a 20 Hz frequency and amplitude of 50 mV. (B) Chronoamperometry response of the L-Dopa biosensor recorded in artificial ISF for increasing L-Dopa levels from 20 to 300 μM with 20 μM increments (from a to o) at 0.3 V vs Ag/AgCl electrode. (Inset shows the corresponding calibration plots). (C) Microneedle sensor stability performance using 100 μM L-Dopa in artificial ISF, 10 repetitive measurements were recorded at each 10 min intervals over a period of 100 min. (D) Operational stability of microneedle TYR biosensor toward 100 μM L-Dopa in artificial ISF over a 100 min period with measurements performed at 10 min intervals.

additions. A well-defined amperometric response is observed over the entire 20−300 μM range. The corresponding calibration plot (shown in the inset) reveals a high linearity over this range with a sensitivity of 0.048 nA/μM. (R^2 = 0.999, n = 3). These obtained responses warrant future possibilities of L-Dopa monitoring in a broad concentration range using tyrosinase-coupled microneedle devices. The L-Dopa microneedle enzymatic sensor offers high reproducibility and stability. The stability test was performed by using a 100 μM L-Dopa in artificial ISF over 110 min periods via repetitive measurements at 10 min intervals. As illustrated in Figure 2D, this experiment resulted in a highly reproducible and stable current response with a standard deviation of 2% (n = 11). Such reproducibility holds promise toward the goal of continuous L-Dopa monitoring.

The detection limit for the L-Dopa sensor was evaluated using the nonenzymatic SWV microneedle sensor in artificial ISF solution containing increasing L-Dopa concentrations between 0.5 and 3 μM (Figure S5A). The optimized SWV parameters (potential range, −0.4 to 1.0 V vs Ag/AgCl using a frequency of 20 Hz and the amplitude of 50 mV) and optimized experimental conditions (1% Nafion: 2 μL, accumulation time: 6 min) were used to perform these experiments. As presented in Figure S5A, well-defined voltammograms were obtained throughout the tested concentration range. The L-Dopa oxidation peak was obtained at a potential of 0.21 V. The corresponding calibration plot for L-Dopa detection was displayed in Figure S5A, inset. Dynamic linear ranges were observed in the concentration range between 0.5 and 3 μM with a correlation coefficient of 0.9875 (RSD 4.5%, n = 3). A detection limit of approximately 0.5 μM was estimated based on the signal-to-noise (S/N = 3) response.

The analytical quantification of the enzymatic microneedle biosensor toward L-Dopa was evaluated by recording chronoamperometry responses in artificial ISF solution having the concentration range between 0.25 and 3 μM (Figure S5B). The current was sampled for 60 s at an applied working potential of 0.3 V versus Ag/AgCl reference electrode. Figure S5B displays a chronoamperogram for increasing the L-Dopa concentrations (0.25 to 3.0 μM) along with the corresponding calibration plot (inset). The entire range of concentrations in well-defined amperograms is observed. The current increases linearly with the increase in the concentration of L-Dopa and a correlation coefficient of 0.999 (RSD = 3.2%, n = 3). A detection limit of approximately 0.25 μM was estimated based on the signal-to-noise (S/N = 3) characteristics of the response.

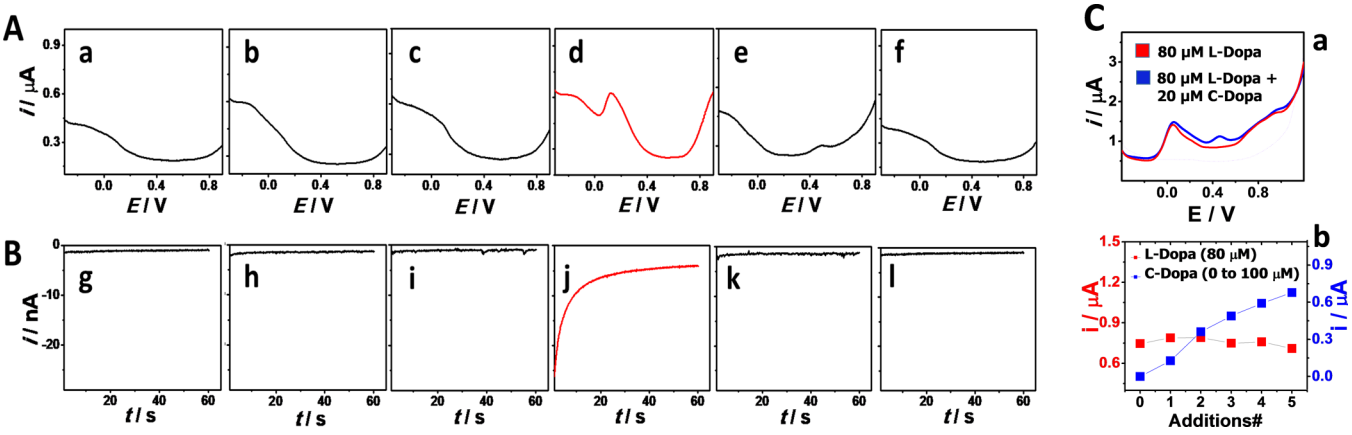

Figure 3. Selectivity of the dual-mode microneedle sensor toward L-Dopa detection in the presence of potential interferences. (A) Square-wave and (B) amperometric responses of the L-Dopa microneedle in artificial ISF; baseline (a, g), ascorbic acid (b, h), uric acid (c, i), L-Dopa (d, j), tyrosine (e, k), and theophylline (f, l). Concentration of L-Dopa is 50 μM, and other interferences are 150 μM; (C) L-Dopa and C-Dopa cross-talk studies. (a) Square-wave voltammograms for 80 μM L-Dopa (red color) and 20 μM C-Dopa + 80 μM L-Dopa (blue color) in artificial ISF. (b) Calibration plots of the background-subtracted peak current vs L-Dopa concentration (red), background-subtracted peak current vs C-Dopa concentration (blue). SWV potential range: −0.4 to 1.0 V (vs Ag/AgCl) using a frequency of 20 Hz and amplitude of 50 mV.

DOI: 10.1021/acssensors.9b01127
ACS Sens. XXXX, XXX, XXX−XXX

Specific detection of the target drug is vital for realizing reliable L-Dopa detection in the presence of potential coexisting interferences. The selectivity of the microneedle sensor array was evaluated by examining the response of both the enzymatic and nonenzymatic microneedle electrodes to possible coexisting interferences, such as ascorbic acid, uric acid, tyrosine, and theophylline using artificial ISF medium (Figure 3). This testing was carried out using 50 μM L-Dopa in the presence of threefold higher concentrations (150 μM) of the potential interfering compounds. As indicated in Figure 3A (a–f), the unmodified microneedle carbon-paste electrode displays a highly selective SWV response in the presence of an excess of all other potential interferences. As illustrated in Figure 3 B (g–l), the enzyme-based microneedle biosensor displays similar high selectivity toward L-Dopa detection with its amperometric response not affected by the presence of these potential interferences. It should be pointed out that operating the nonenzymatic paste microneedle amperometrically (at +0.2 V) instead of the SWV mode offered also selective detection of L-Dopa in the presence of these interferences (not shown). In all cases, the high selectivity of these microneedle sensors reflects the combination of a low operating potential with a perm-selective Nafion layer that rejects negatively charged species such as ascorbic acid and uric acid (along with the specific biocatalytic reaction in the case of the enzyme microneedle sensor).

C-Dopa is an important administrated drug, often used as an inhibitor in PD therapeutic applications along with L-Dopa with the control ratio of 4:1 (L-Dopa:C-Dopa). C-Dopa is mainly useful to reduce side effects of L-Dopa and subsequently improves the efficiency of therapy, which leads to the better control of PD. Hence, it is important to examine the influence of C-Dopa upon the L-Dopa response. Here, the orthogonal detection is advantageous as the enzyme-based sensor responds to both drugs. In contrast, the nonenzymatic SWV microneedle sensor allows simultaneous detection of L-Dopa and C-Dopa. L-Dopa and C-Dopa cross studies were thus conducted using the unmodified CP microneedle sensor in artificial ISF to evaluate distinct detection of both analytes (Figure 3C). Upon testing 80 μM L-Dopa, a clear and distinct SWV was observed at 0.1 V; subsequent addition of 20 μM C-Dopa resulted in two separate peaks at 0.1 V and 0.5 V for L-Dopa and C-Dopa, respectively. Later, we have carried out the calibration studies of C-Dopa in a varied concentration range between 0 and 100 μM in the presence of L-Dopa (80 μM). The C-Dopa SWV current values were increased linearly with respective additions of concentrations without affecting the current values of L-Dopa (Figure 3C). Such high selectivity of L-Dopa in the presence of C-Dopa reflects that the proposed microneedle-sensing platform offers significant promise for the monitoring of PD.

Dual L-Dopa Microneedle Sensing: Phantom-Gel Mimicked Skin Model Evaluation, ex Vivo Mice Skin, and Stability in the Presence of Proteins. After the successful evaluation of individual enzymatic and non-enzymatic microneedle sensors using the different electrochemical techniques (SWV and chronoamperometry), we have tested the microneedles by interchanging working sensors alternatively to detect L-Dopa in artificial ISF. The SWV and chronoamperometry experiments were carried out simultaneously on three CP-modified microneedle electrodes. The SWV and the chronoamperometric response of both microneedle sensors were recorded simultaneously upon adding 50 μM L-Dopa to artificial ISF (Figure 4A,B). Both microsensors WE1 and WE2 display a well-defined response with current

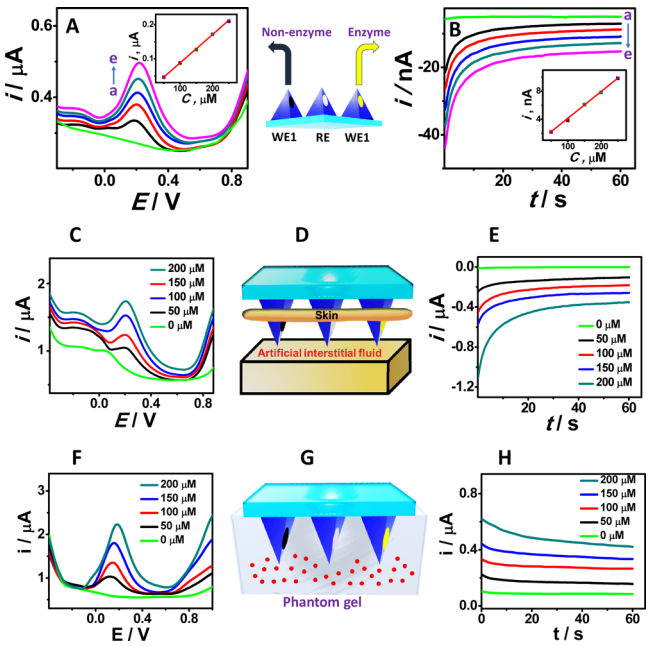

Figure 4. (A) square-wave voltammograms for L-Dopa in ISF from 50 to 250 μM concentrations in 50 μM increments. (Inset shows the calibration plot of the background-subtracted peak-current vs L-Dopa concentration). (B) Chronoamperometry responses of the L-Dopa biosensor recorded in ISF from 50 to 250 μM in 20 μM increments at 0.3 V vs Ag/AgCl electrode. (Inset shows the corresponding calibration plots.) (C, E) Real-time L-Dopa detection in artificial ISF through the mice skin-penetrated microneedle. (F, H) SWV and amperometric responses of different L-Dopa concentrations with the mimicking-skin phantom gel. (D) Schematic showing the detection of L-Dopa in artificial ISF using the microneedle penetrated through the mice skin. (G) Schematic representation of the mimicking-skin phantom gel with the penetration of the microneedle. Other conditions are as in Figure 2.

signals proportional to the L-Dopa concentration. Such linearity is indicated from the corresponding calibration plots (see insets) with correlation coefficients of 0.998 and 0.999 (RSD = 3%) with the sensitivity of 0.082 μA/μM and 0.038 nA/μM for the SWV and amperometric signals, respectively.

The analytical performance of the microneedle sensor array was assessed for L-Dopa detection in artificial ISF in connection to an ex vivo mice skin model. As shown in Figure 4D, the microneedle sensor was pierced onto the mice skin to access the target ISF L-Dopa. The L-Dopa level in the artificial ISF compartment was thus increased linearly between 50 and 200 μM, and the corresponding SWV (nonenzyme) and chronoamperometric (enzymatic) measurements were carried out simultaneously. A distinct and well-defined voltammetric and amperometric L-Dopa response, proportional to the drug concentration, is observed, reflecting the suitability of both microneedle electrodes for such through skin sensing (Figure 4C,E). To mimic future monitoring of PD patients, the microneedle sensor array was evaluated using a tissue (dermis)-mimicking phantom gel skin model involving an agarose (1.4%) hydrogel (Figure 4G). The microneedle sensor array with its electrode tips is located inside the gel. As illustrated in Figure 4F,H, the phantom-gel experiment yielded well-defined voltammetric and amperometric responses for the

DOI: 10.1021/acssensors.9b01127
ACS Sens. XXXX, XXX, XXX–XXX

increasing L-Dopa gel concentrations in 50 μM steps. Overall, such favorable responses of both the ex vivo skin model and the tissue-mimicking phantom-gel results hold considerable promise toward future continuous in vivo L-Dopa monitoring.

Minimally invasive ISF monitoring is commonly subject to surface biofouling due to protein constituents of the ISF. To address such biofouling effects, the surface of our microneedle electrodes has been coated with a protective Nafion film. As illustrated in Figure S6, the sensor stability was tested in the presence of common ISF proteins,[48,49] 2 mg mL^{-1} albumin and 0.5 mg mL^{-1} γ-globulin. Both tested microneedle sensors displayed a relatively stable response for repetitive measurements at 10 min intervals over a 2 h period. Despite the presence of the protein fouling agents, only an 11 and 14% decrease of the response of the nonenzymatic and enzymatic microneedle sensors, respectively, were observed over the entire 2 h experimental period. Current efforts are aimed at minimizing further the protection against biofouling through the combination of additional protective coatings.

CONCLUSIONS

We have demonstrated the first example of a wearable chemical sensing platform based on a microneedle electrode array for continuous monitoring of the antiparkinsonian drug L-Dopa and introduced a new dual-mode sensing approach based on independent electrochemical measurements involving redox and biocatalytic processes. Such multimodal L-Dopa sensing offers a built-in redundancy and enhances the information content of the microneedle sensor arrays. The new orthogonal microneedle sensing relies on the simultaneous L-Dopa sensing by SWV and chronoamperometry measurements at unmodified and enzyme-modified carbon-paste electrodes, respectively. The resulting microneedle sensing platform displays an attractive analytical performance in skin-mimicking phantom gel as well as upon penetration through mice skin with high sensitivity, a wide linear dynamic range, and good stability along with high selectivity. The ability to combine several distinct independent processes onto a single wearable platform holds considerable potential for enhancing the power of a wide range of on-body chemical sensing devices in general and could be readily extended to the monitoring of other key biomarkers in different biofluids.

Overall, such a dual-mode microneedle L-Dopa sensing platform holds considerable promise for providing timely feedback on a proper L-Dopa dosing regimen in a decentralized fashion. Such effective real-time L-Dopa monitoring capability would allow optimal dosing and improved management of PD. These developments represent the first step toward addressing the urgent need for effective L-Dopa monitoring. Future efforts toward on-body testing will assess the biocompatibility of the microneedle sensors and particularly of the carbon-paste transducer and will assess other carbon electrode materials. While conventional carbon-paste microelectrodes have been widely used for in vivo brain monitoring, recent efforts in our laboratory have demonstrated a variety of paste electrode materials based on fully edible oil binders, such as olive oil.[50,51] Future efforts will aim also at establishing the correlation between the L-Dopa concentration in blood and the ISF. While small analytes interchange freely between these biofluids by diffusion, such a relationship may depend on the half-life of the drug.[52] The influence of the microneedle geometry upon the spatiotemporal variations of the measured L-Dopa concentration should also be considered.[53] Future efforts will focus also on the full integration of the wireless electronic interface and wireless transmission, investigation of effective antibiofouling protecting coatings, and clinical testing and validation in PD patients. Eventually, these advances will lead to a closed-loop system, containing an L-Dopa pump and a dose-automation algorithm, which will replace the common intermittent oral administration toward optimal individualized drug dosing and a greatly improved management of PD symptoms.

ASSOCIATED CONTENT

Supporting Information

The Supporting Information is available free of charge on the ACS Publications website at DOI: 10.1021/acssensors.9b01127.

SWV operation and chronoamperometric responses (PDF)

AUTHOR INFORMATION

Corresponding Authors

*E-mail: ilitvan@ucsd.edu (I.L.).
*E-mail: josephwang@ucsd.edu (J.W.).

Notes

The authors declare no competing financial interest.

ACKNOWLEDGMENTS

I.L. is supported by the National Institutes of Health (grant nos. 5P50AG005131-33, 2R01AG038791-06A, U01NS090259, 1U54 NS 092089, U01NS100610, U01NS80818, R25NS098999, and P20GM109025), Parkinson Study Group, Michael J Fox Foundation, Lewy Body Association, AVID Pharmaceuticals, Abbvie, Biogen, and Roche. C.M. acknowledges the Science Achievement Scholarship of Thailand (SAST) for financial support.

REFERENCES

(1) Berg, D.; Postuma, R. B.; Adler, C. H.; Bloem, B. R.; Chan, P.; Dubois, B.; Gasser, T.; Goetz, C. G.; Halliday, G.; Joseph, L.; et al. MDS Research Criteria for Prodromal Parkinson's Disease. *Mov. Disord.* **2015**, *30*, 1600−1611.

(2) Pringsheim, T.; Jette, N.; Frolkis, A.; Steeves, T. D. L. The Prevalence of Parkinson's Disease: A Systematic Review and Meta-Analysis. *Mov. Disord.* **2014**, *29*, 1583−1590.

(3) Marras, C.; Beck, J. C.; Bower, J. H.; Roberts, E.; Ritz, B.; Ross, G. W.; Abbott, R. D.; Savica, R.; Van Den Eeden, S. K.; Willis, A. W.; et al. Prevalence of Parkinson's Disease across North America. *npj Parkinson's Dis.* **2018**, *4*, 21.

(4) Lin, L.; Lian, H.-T.; Sun, X.-Y.; Yu, Y.-M.; Liu, B. An l-dopa Electrochemical Sensor Based on a Graphene Doped Molecularly Imprinted Chitosan Film. *Anal. Methods* **2015**, *7*, 1387−1394.

(5) Postuma, R. B.; Berg, D.; Stern, M.; Poewe, W.; Olanow, C. W.; Oertel, W.; Obeso, J.; Marek, K.; Litvan, I.; Lang, A. E.; et al. MDS Clinical Diagnostic Criteria for Parkinson's Disease. *Mov. Disord.* **2015**, *30*, 1591−1601.

(6) Agid, Y. Levodopa. Is Toxicity a Myth? *Neurology* **1998**, *50*, 858−863.

(7) Fabbrini, G.; Juncos, J.; Mouradian, M. M.; Serrati, C.; Chase, T. N. Levodopa Pharmacokinetic Mechanisms and Motor Fluctuations in Parkinson's Disease. *Ann. Neurol.* **1987**, *21*, 370−376.

(8) Nyholm, D.; Lennernäs, H.; Gomes−Trolin, C.; Aquilonius, S.-M. Levodopa Pharmacokinetics and Motor Performance During Activities of Daily Living in Patients With Parkinson's Disease on Individual Drug Combinations. *Clin. Neuropharmacol.* **2002**, *25*, 89−96.

DOI: 10.1021/acssensors.9b01127
ACS Sens. XXXX, XXX, XXX−XXX

(9) Blandini, F.; Martignoni, E.; Pacchetti, C.; Desideri, S.; Rivellini, D.; Nappi, G. Simultaneous Determination of L-Dopa and 3-O-Methyldopa in Human Platelets and Plasma Using High-Performance Liquid Chromatography with Electrochemical Detection. *J. Chromatogr. B: Biomed. Sci. Appl.* **1997**, *700*, 278−282.
(10) Babaei, A.; Babazadeh, M. A Selective Simultaneous Determination of Levodopa and Serotonin Using a Glassy Carbon Electrode Modified with Multiwalled Carbon Nanotube/Chitosan Composite. *Electroanalysis* **2011**, *23*, 1726−1735.
(11) Brunetti, B.; Valdés-Ramírez, G.; Litvan, I.; Wang, J. A Disposable Electrochemical Biosensor for L-DOPA Determination in Undiluted Human Serum. *Electrochem. Commun.* **2014**, *48*, 28−31.
(12) Yan, X.-X.; Pang, D.-W.; Lu, Z.-X.; Lü, J.-Q.; Tong, H. Electrochemical Behavior of L-Dopa at Single-Wall Carbon Nanotube-Modified Glassy Carbon Electrodes. *J. Electroanal. Chem.* **2004**, *569*, 47−52.
(13) Shahrokhian, S.; Asadian, E. Electrochemical Determination of L-Dopa in the Presence of Ascorbic Acid on the Surface of the Glassy Carbon Electrode Modified by a Bilayer of Multi-Walled Carbon Nanotube and Poly-Pyrrole Doped with Tiron. *J. Electroanal. Chem.* **2009**, *636*, 40−46.
(14) Babaei, A.; Sohrabi, M.; Afrasiabi, M. A Sensitive Simultaneous Determination of Epinephrine and Piroxicam Using a Glassy Carbon Electrode Modified with a Nickel Hydroxide Nanoparticles/Multi-walled Carbon Nanotubes Composite. *Electroanalysis* **2012**, *24*, 2387−2394.
(15) Yue, H. Y.; Zhang, H.; Huang, S.; Gao, X.; Chang, J.; Lin, X. Y.; Yao, L. H.; Wang, L. P.; Guo, E. J. Selective Determination of L-Dopa in the Presence of Ascorbic Acid and Uric Acid Using a 3D Graphene Foam. *J. Solid State Electrochem.* **2018**, *22*, 3527−3533.
(16) Arvand, M.; Ghodsi, N. Electrospun TiO_2 Nanofiber/Graphite Oxide Modified Electrode for Electrochemical Detection of l-DOPA in Human Cerebrospinal Fluid. *Sens. Actuators, B* **2014**, *204*, 393−401.
(17) Prabhu, P.; Suresh Babu, R.; Sriman Narayanan, S. Amperometric Determination of L-Dopa by Nickel Hexacyanoferrate Film Modified Gold Nanoparticle Graphite Composite Electrode. *Sens. Actuators, B* **2011**, *156*, 606−614.
(18) Kim, J.; Campbell, A. S.; de Ávila, B. E.-F.; Wang, J. Wearable Biosensors for Healthcare Monitoring. *Nat. Biotechnol.* **2019**, *37*, 389−406.
(19) Kim, J.; Jeerapan, I.; Sempionatto, J. R.; Barfidokht, A.; Mishra, R. K.; Campbell, A. S.; Hubble, L. J.; Wang, J. Wearable Bioelectronics: Enzyme-Based Body-Worn Electronic Devices. *Acc. Chem. Res.* **2018**, *51*, 2820−2828.
(20) Campbell, A. S.; Kim, J.; Wang, J. Wearable Electrochemical Alcohol Biosensors. *Curr. Opin. Electrochem.* **2018**, *10*, 126−135.
(21) Miller, P. R.; Narayan, R. J.; Polsky, R. Microneedle-Based Sensors for Medical Diagnosis. *J. Mater. Chem. B* **2016**, *4*, 1379−1383.
(22) Tasca, F.; Tortolini, C.; Bollella, P.; Antiochia, R. Microneedle-based Electrochemical Devices for Transdermal Biosensing: a Review. *Curr. Opin. Electrochem.* **2019**, *16*, 42−49.
(23) Wang, M.; Hu, L.; Xu, C. Recent Advances in the Design of Polymeric Microneedles for Transdermal Drug Delivery and Biosensing. *Lab Chip* **2017**, *17*, 1373−1387.
(24) Patel, S.; Lorincz, K.; Hughes, R.; Huggins, N.; Growdon, J.; Standaert, D.; Akay, M.; Dy, J.; Welsh, M.; Bonato, P. Monitoring Motor Fluctuations in Patients With Parkinson's Disease Using Wearable Sensors. *IEEE Trans. Inf. Technol. Biomed.* **2009**, *13*, 864−873.
(25) Ma, G.; Wu, C. Microneedle, Bio-Microneedle and Bio-Inspired Microneedle: A Review. *J. Controlled Release* **2017**, *251*, 11−23.
(26) Ventrelli, L.; Marsilio Strambini, L.; Barillaro, G. Microneedles for Transdermal Biosensing: Current Picture and Future Direction. *Adv. Healthcare Mater.* **2015**, *4*, 2606−2640.
(27) Bhatnagar, S.; Dave, K.; Venuganti, V. V. K. Microneedles in the Clinic. *J. Controlled Release* **2017**, *260*, 164−182.
(28) Kim, K. B.; Lee, W.-C.; Cho, C.-H.; Park, D.-S.; Cho, S. J.; Shim, Y.-B. Continuous Glucose Monitoring Using a Microneedle Array Sensor Coupled with a Wireless Signal Transmitter. *Sensors Actuators B Chem.* **2019**, *281*, 14−21.
(29) Lee, S. J.; Yoon, H. S.; Xuan, X.; Park, J. Y.; Paik, S.-J.; Allen, M. G. A Patch Type Non-Enzymatic Biosensor Based on 3D SUS Micro-Needle Electrode Array for Minimally Invasive Continuous Glucose Monitoring. *Sensors Actuators B Chem.* **2016**, *222*, 1144−1151.
(30) Lee, H.; Choi, T. K.; Lee, Y. B.; Cho, H. R.; Ghaffari, R.; Wang, L.; Choi, H. J.; Chung, T. D.; Lu, N.; Hyeon, T.; et al. A Graphene-Based Electrochemical Device with Thermoresponsive Microneedles for Diabetes Monitoring and Therapy. *Nat. Nanotechnol.* **2016**, *11*, 566−572.
(31) Chinnadayyala, S. R.; Park, I.; Cho, S. Nonenzymatic Determination of Glucose at near Neutral PH Values Based on the Use of Nafion and Platinum Black Coated Microneedle Electrode Array. *Microchim. Acta* **2018**, *185*, 250.
(32) Li, C. G.; Joung, H.-A.; Noh, H.; Song, M.-B.; Kim, M.-G.; Jung, H. One-Touch-Activated Blood Multidiagnostic System Using a Minimally Invasive Hollow Microneedle Integrated with a Paper-Based Sensor. *Lab Chip* **2015**, *15*, 3286−3292.
(33) Jina, A.; Tierney, M. J.; Tamada, J. A.; McGill, S.; Desai, S.; Chua, B.; Chang, A.; Christiansen, M. Design, Development, and Evaluation of a Novel Microneedle Array-Based Continuous Glucose Monitor. *J. Diabetes Sci. Technol.* **2014**, *8*, 483−487.
(34) Valdés-Ramírez, G.; Li, Y.-C.; Kim, J.; Jia, W.; Bandodkar, A. J.; Nuñez-Flores, R.; Miller, P. R.; Wu, S.-Y.; Narayan, R.; Windmiller, J. R.; et al. Microneedle-Based Self-Powered Glucose Sensor. *Electrochem. Commun.* **2014**, *47*, 58−62.
(35) Samavat, S.; Lloyd, J.; O'Dea, L.; Zhang, W.; Preedy, E.; Luzio, S.; Teng, K. S. Uniform Sensing Layer of Immiscible Enzyme-Mediator Compounds Developed via a Spray Aerosol Mixing Technique towards Low Cost Minimally Invasive Microneedle Continuous Glucose Monitoring Devices. *Biosens. Bioelectron.* **2018**, *118*, 224−230.
(36) Sharma, S.; Huang, Z.; Rogers, M.; Boutelle, M.; Cass, A. E. G. Evaluation of a Minimally Invasive Glucose Biosensor for Continuous Tissue Monitoring. *Anal. Bioanal. Chem.* **2016**, *408*, 8427−8435.
(37) Invernale, M. A.; Tang, B. C.; York, R. L.; Le, L.; Hou, D. Y.; Anderson, D. G. Microneedle Electrodes Toward an Amperometric Glucose-Sensing Smart Patch. *Adv. Healthcare Mater.* **2014**, *3*, 338−342.
(38) Caliò, A.; Dardano, P.; Di Palma, V.; Bevilacqua, M. F.; Di Matteo, A.; Iuele, H.; De Stefano, L. Polymeric Microneedles Based Enzymatic Electrodes for Electrochemical Biosensing of Glucose and Lactic Acid. *Sensors Actuators B Chem.* **2016**, *236*, 343−349.
(39) Bollella, P.; Sharma, S.; Cass, A. E. G.; Antiochia, R. Microneedle-Based Biosensor for Minimally-Invasive Lactate Detection. *Biosens. Bioelectron.* **2019**, *123*, 152−159.
(40) Windmiller, J. R.; Zhou, N.; Chuang, M.-C.; Valdés-Ramírez, G.; Santhosh, P.; Miller, P. R.; Narayan, R.; Wang, J. Microneedle Array-Based Carbon Paste Amperometric Sensors and Biosensors. *Analyst* **2011**, *136*, 1846−1851.
(41) Bollella, P.; Sharma, S.; Cass, A.E.G.; Antiochia, R. Minimally-invasive Microneedle-based Biosensor array for Simultaneous Lactate and Glucose Monitoring in Artificial Interstitial Fluid. *Electroanalysis* **2019**, *31*, 374−382.
(42) Mohan, A. M. V.; Windmiller, J. R.; Mishra, R. K.; Wang, J. Continuous Minimally-Invasive Alcohol Monitoring Using Microneedle Sensor Arrays. *Biosens. Bioelectron.* **2017**, *91*, 574−579.
(43) Miller, P. R.; Xiao, X.; Brener, I.; Burckel, D. B.; Narayan, R.; Polsky, R. Microneedle-Based Transdermal Sensor for On-Chip Potentiometric Determination of K +. *Adv. Healthcare Mater.* **2014**, *3*, 876−881.
(44) Mishra, R. K.; Vinu Mohan, A. M.; Soto, F.; Chrostowski, R.; Wang, J. A Microneedle Biosensor for Minimally-Invasive Transdermal Detection of Nerve Agents. *Analyst* **2017**, *142*, 918−924.
(45) Bretag, A. H. Synthetic Interstial Fluid for Isolated Mammalian Tissue. *Life Sci.* **1969**, *8*, 319−329.

DOI: 10.1021/acssensors.9b01127
ACS Sens. XXXX, XXX, XXX−XXX

(46) Chang, H.; Zheng, M.; Yu, X.; Than, A.; Seeni, R. Z.; Kang, R.; Tian, J.; Khanh, D. P.; Liu, L.; Chen, P.; et al. A Swellable Microneedle Patch to Rapidly Extract Skin Interstitial Fluid for Timely Metabolic Analysis. *Adv. Mater.* **2017**, *29*, 1702243.
(47) Gao, Y.; Hou, M.; Yang, R.; Zhang, L.; Xu, Z.; Kang, Y.; Xue, P. PEGDA/PVP Microneedles with Tailorable Matrix Constitutions for Controllable Transdermal Drug Delivery. *Macromol. Mater. Eng.* **2018**, *303*, 1800233.
(48) Fogh-Andersen, N.; Altura, B. M.; Altura, B. T.; Siggaard-Andersen, O. Composition of Interstitial Fluid. *Clin. Chem.* **1995**, *41*, 1522−1525.
(49) Gilanyi, M.; Ikrenyi, C.; Fekete, J.; Ikrenyi, K.; Kovach, A. G. Ion Concentrations in Subcutaneous Interstitial Fluid: Measured versus Expected Values. *Am. J. Physiol. Physiol.* **1988**, *255*, F513−F519.
(50) Kim, J.; Jeerapan, I.; Ciui, B.; Hartel, M. C.; Martin, A.; Wang, J. Edible Electrochemistry: Food Materials Based Electrochemical Sensors. *Adv. Healthcare Mater.* **2017**, *6*, 1700770.
(51) Jeerapan, I.; Ciui, B.; Martin, I.; Cristea, C.; Sandulescu, R.; Wang, J. Fully Edible Biofuel Cells. *J. Mater. Chem. B* **2018**, *6*, 3571−3578.
(52) Heikenfeld, J.; Jajack, A.; Feldman, B.; Granger, S.W.; Gaitonde, S.; Begtrup, G.; Katchman, B. A. Accessing Analytes in Biofluids for Peripheral Biochemical Monitoring. *Nat. Biotechnol.* **2019**, *37*, 407−419.
(53) Miller, P. R.; Taylor, R. M.; Tran, B. Q.; Boyd, G.; Glaros, T.; Chavez, V. H.; Krishnakumar, R.; Sinha, A.; Poorey, K.; Williams, K. P.; et al. Extraction and Biomolecular Analysis of Dermal Interstitial Fluid Collected with Hollow Microneedles. *Commun. Biol.* **2018**, *1*, 173.

DOI: 10.1021/acssensors.9b01127
ACS Sens. XXXX, XXX, XXX−XXX